

Aluminum corrosion–passivation regulation prolongs aqueous batteries life

Received: 15 July 2023

Accepted: 21 March 2024

Published online: 04 April 2024

Check for updates

Binghang Liu^{1,2,3}, Tianshi Lv^{1,2,3}, Anxing Zhou^{1,2,3}, Xiangzhen Zhu^{1,2,3}, Zejing Lin^{1,2}, Ting Lin¹ & Liumin Suo^{1,2,3}✉

Aluminum current collectors are widely used in nonaqueous batteries owing to their cost-effectiveness, lightweightness, and ease of fabrication. However, they are excluded from aqueous batteries due to their severe corrosion in aqueous solutions. Here, we propose hydrolyzation-type anodic additives to form a robust passivation layer to suppress corrosion. These additives dramatically lower the corrosion current density of aluminum by nearly three orders of magnitude to $\sim 10^{-6}$ A cm⁻². In addition, realizing that electrochemical corrosion accompanies anode prelithiation, we propose a prototype of self-prolonging aqueous Li-ion batteries (Al || LiMn₂O₄ || TiO₂), whose capacity retention rises from 49.5% to 70.1% after 200 cycles. A sacrificial aluminum electrode where electrochemical corrosion is utilized is introduced as an electron supplement to prolong the cycling life of aqueous batteries. Our work addresses the short-life issue of aqueous batteries resulting from the corrosion of the current collector and lithium loss from side reactions.

Aqueous Li-ion batteries (ALIBs) show promise as large-scale energy storage technology due to their nonflammability and environmental friendliness^{1–6}. However, their cycle life is inadequate for the demand in energy storage due to irreversible parasitic side reactions from their cathode and anode sides.

The cathode side expectedly features cycling fading in the form of irreversible oxidation corrosion of metal current collectors in aqueous electrolytes^{4,6–9}. Thus, cost-effective, manufacture-friendly, and lightweight Al foils are excluded as current collectors in ALIBs because of the harsh aqueous environment attacks on the Al₂O₃ passivation film and continuous corrosion of Al, which damage the electronic matrix and result in contact loss and high resistance of electrodes¹⁰. To address these issues, scholars have used durable metal current collectors, including titanium¹¹, nickel¹², stainless steel^{3,9}, and carbon foil^{13–17}, to reduce the effects of corrosion on ALIBs. However, almost all of these candidates fail as substitutes to Al current collectors, which can simultaneously satisfy the lightweight, conductivity, mechanical strength, and cost-effectiveness requirements.

Different from nonaqueous electrolytes that passivate Al through the addition of effective salts, such as LiPF₆, LiBF₄, LiDFOB, or

optimization of solvents with a low dielectric constant^{10,18–28}, the passivation of Al metal foil in aqueous solutions is considerably more challenging because of the incompatibility of the salts and water. On the one hand, solvent water possesses a relatively high dielectric constant (78.4 F m⁻¹ at 25 °C), which promotes the diffusion of corrosion products and accelerates Al corrosion^{18,19}; on the other hand, the formation of solid electrolyte interphase (SEI) in aqueous electrolytes highly depends on organic salts, such as bis(trifluoromethane sulfonyl) imide (LiTFSI), and lithium trifluoromethanesulfonate (LiOTF)³, whose anions are aggressive against Al regardless of the use of nonaqueous or aqueous electrolytes^{18–20,26–29}. Therefore, addressing the corrosion of Al by aqueous LiTFSI electrolyte poses an important challenge in the field of aqueous batteries. Although the corrosion of Al current collectors can be suppressed through the increase in salt concentration^{4,6} since high concentration and high viscosity decrease the dissolving capability and hinder the departure of corrosion products from the of Al surface^{4,6,20–22}, high concentration also increases the cost against the original intention of employing low-cost Al current collectors.

From the anode side, another failure mechanism of cycling life results from lithium loss caused by the formation of a SEI and

¹Beijing National Laboratory for Condensed Matter Physics, Institute of Physics, Chinese Academy of Science, 100190 Beijing, China. ²Center of Materials Science and Optoelectronics Engineering, University of Chinese Academy of Sciences, 100049 Beijing, China. ³Yangtze River Delta Physics Research Center Co. Ltd, 213300 Liyang, China. ✉e-mail: suoliumin@iphy.ac.cn

hydrogen evolution reaction (HER), which lead to a rapid capacity degradation. Typically, SEI formation in traditional nonaqueous LIBs irreversibly consumes 6%–15% Li ions, which are extracted from the cathode material, and reduces the specific energy by 5%–20% during the initial cycle^{30,31}. However, as the extra HER that consumes the Li resource does not contribute to SEI formation, irreversible Li consumption is expectedly more severe in ALIBs^{5,32}; this condition results in a high P/N (cathode-to-anode mass ratio) > 1.5, which offsets the lithium compensation for the capacity loss from HER and SEI.

Based on the above information, the critical challenge in ALIB application is the stabilization of the Al current collector in low-concentration aqueous electrolytes. Here, we proposed a prolonged life strategy for aqueous batteries that involves the electrochemical regulation of the corrosion and passivation of Al to make it an electron supplement and a stable current collector. We used the hydrolyzation type-anodic additive (HTA) to achieve electrochemical–chemical passivation of the Al current collector and successfully precipitated Al(OH)₃ as a passivating layer on the Al surface. In addition, the passivation process, which involves Al oxidation at the cathode, can supplement electrons to anode, which promotes the compensation of the capacity loss resulting from hydrogen evolution at the anode side. The oxidation of Al is an electron supplement process, with an additional lithium source originating from the electrolyte as supplement. Therefore, in this context, an “electron supplement” was used instead of “lithium supplement.” Furthermore, considering practical industrial applications, we designed a prototype of self-prolonging ALIBs (SP-ALIBs) (Al||LiMn₂O₄||TiO₂) with an Al-sacrificing electrode, which enabled self-lithium supplementation via periodic switching between either full LiMn₂O₄||TiO₂ or Al||TiO₂ in combination with electrochemical regulation.

Results

Design of Al-passivating additives in an aqueous electrolyte

Figure 1 illustrates the schematic of our proposed HTA-passivating mechanism for Al current collectors in aqueous LiTFSI electrolytes. As reported previously^{18,26}, TFSI⁻ aggressively destroys the original Al₂O₃ layer to form dissolved [Al(TFSI)_x^{3-x}] at the initial active spots of the Al surface film (TFSI⁻(aq) + Al₂O₃ → Al(TFSI)_x^{3-x}(aq) + O₂ + e⁻). Then, more active spots emerged, which caused pitting corrosion (Al(s) - e⁻ + TFSI⁻(aq) → Al(TFSI)_x^{3-x}(aq)). Therefore, given the inevitability of attacks from TFSI⁻ to the original passivation Al₂O₃ layer, our design principle was aimed at the chemical conversion of the initial electrochemical corrosion product to insoluble solid-phase aluminum compounds and coverage of the Al surface as a passivation layer. Previous

literature proposed the protection of Al from chloride corrosion through the construction of inorganic passivation layers^{33,34}. Given this information, some insoluble aluminum compounds (Al₃M₆), such as Al(OH)₃, can serve as target passivation products due to their relatively low solubility product constant; studies have reported the corrosion resistance of these compounds against chloride ions^{34,35}. We applied the universal corrosion principles in aqueous batteries to prevent the Al current collector from being corroded by TFSI⁻. To form a robust and dense Al₃M₆ layer and restore the passivation layer on the Al surface, we contemplated on the use of Al ions generated by electrochemical corrosion during battery charging (Al(s) - e⁻ → Al³⁺) to chemically transform Al into solid-phase depositions and form a passivation layer (reaction path: Al(s) - e⁻ + H_xMⁿ⁺(aq) + H₂O → Al(OH)₃(s) + H_{x+1}M¹⁻ⁿ(aq)) instead of dissolution in electrolytes as [Al(TFSI)_x^{3-x}]. First, electrochemical corrosion occurs, followed by chemical passivation that is, electrochemical–chemical passivation. Based on preceding findings, slightly soluble lithium weak acid salts, such as Li₃PO₄, Li₂CO₃, Li₂SiO₃, and LiAlO₂, were proposed as passivation additives for Al in aqueous electrolytes, whose anions after hydrolysis can combine with proton. These salts also perform a function similar to pH buffers in proximity to the Al foil and facilitate the formation of Al(OH)₃. Supplementary Information Note 2 provides a detailed discussion on the role of HTA.

To verify the anticorrosion effectiveness of HTA, we performed CA experiments using LiTFSI solution on three-electrode devices (Al-WE||Ag/AgCl-RE||Al-CE), where the potential of Al-WE was set at 4.5 V vs Li/Li⁺ for 10 minutes and then relaxed to the open-circuit potential (OCV) for 1 minute, for a total of 12 cycles (Fig. 2A). This periodic switching between 4.5 V and OCV eliminated the effect on transport limitations at the interface, which ensured that the experiment proceeded under harsh conditions. HTAs (Li₃PO₄, Li₂CO₃, LiAlO₂, and Li₂SiO₃) were added to 1 and 10 m LiTFSI solutions, whose content was saturated (<0.05 m). Al in the blank electrolyte (1 m LiTFSI) had a corrosion current density extremely higher than 10⁻³ A cm⁻², which indicates its severe corrosion in the diluted solution (Fig. 2A). Notably, after the introduction of saturated LiAlO₂, Li₂CO₃, and Li₃PO₄, the corrosion current density dropped dramatically by nearly three orders of magnitude (10⁻⁶ A cm⁻²), which indicates a satisfying anticorrosion effectiveness. The CA experiments (Fig. 2A, B) were repeated twice to verify our claims (Figs. S7 and S8, respectively). Moreover, Supplementary Information Note 2 discusses the influence of the HTA amount on corrosion resistance.

To further support our claim, we used inductive coupled plasma (ICP) to detect the dissolved Al ion content in the electrolyte and

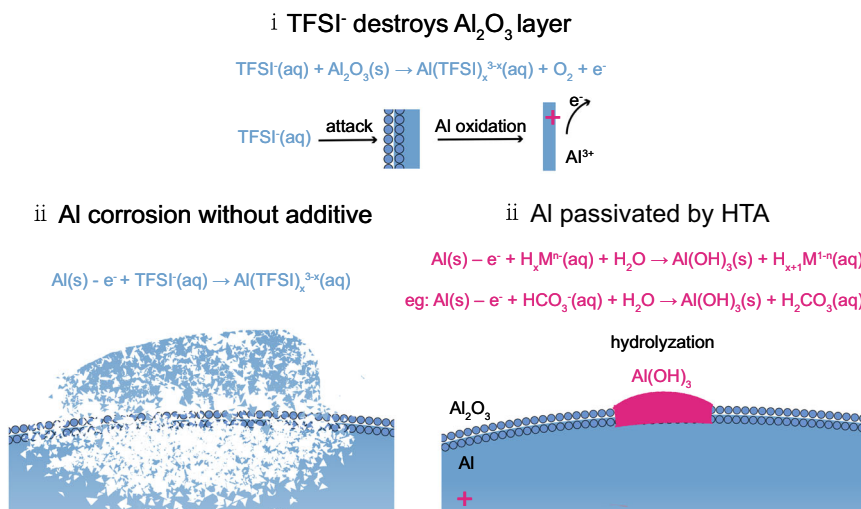


Fig. 1 | How TFSI⁻ corrodes Al and HTA passivates Al. Schematic of HTA-passivating Al mechanism in an aqueous LiTFSI electrolyte.

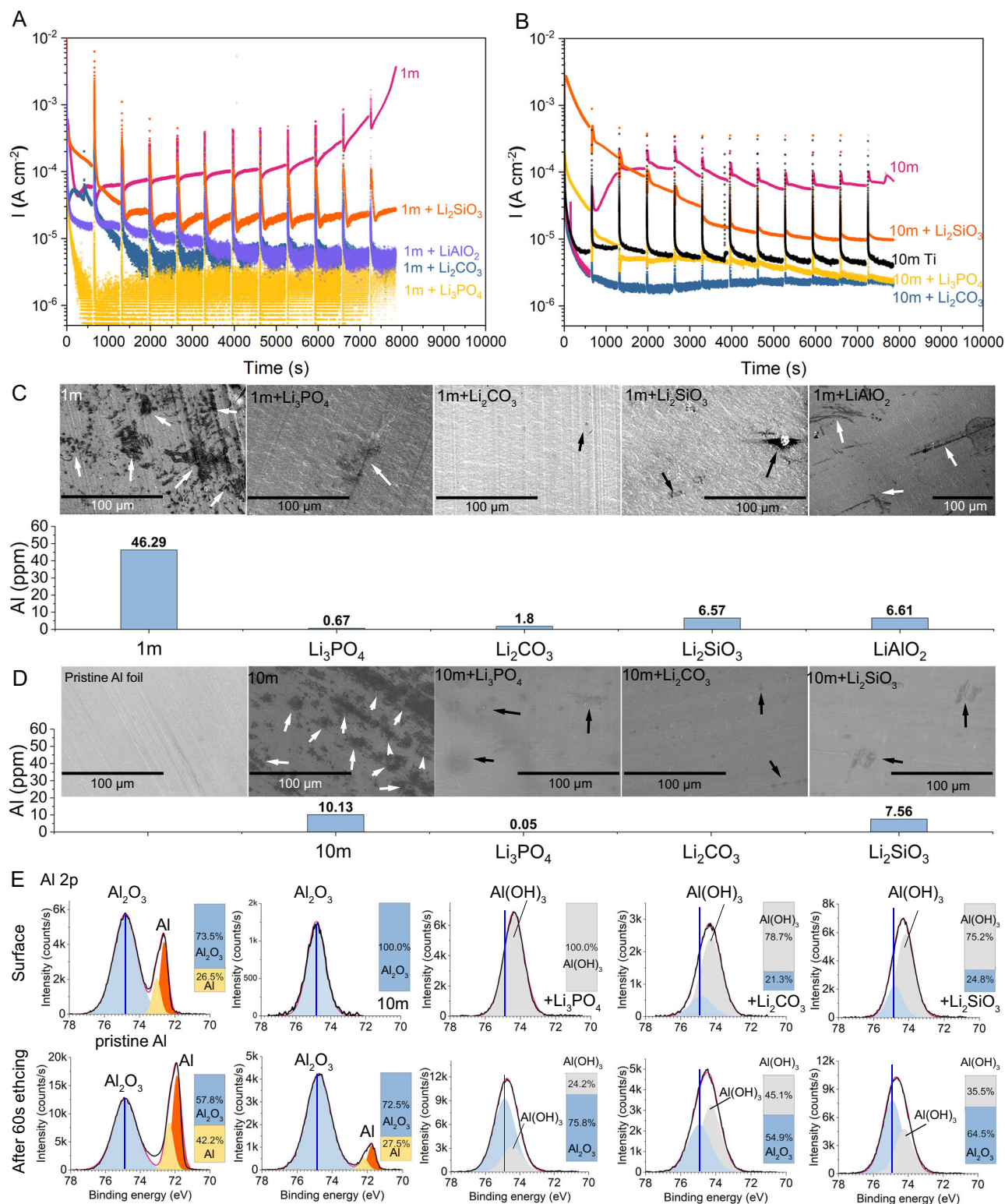


Fig. 2 | Anticorrosion effect of HTA on the Al current collector.

A, B Chronoamperometry (CA) experiments in 1 and 10 m LiTFSI solutions with saturated HTA (Li₃PO₄, Li₂CO₃, LiAlO₂, and Li₂SiO₃). **C, D** Al contents in electrolytes obtained via inductive coupled plasma (ICP) measurement and SEM images of Al

foils after CA experiments using 1 and 10 m LiTFSI solutions with HTA. **E** Al 2p X-ray photoelectron spectroscopy (XPS) spectra of Al foil after CA experiments using 10 m LiTFSI with HTA before and after 60 s Ar⁺ sputtering. The blue vertical line is based on the Al₂O₃ peak of pristine Al.

scanning electron microscopy (SEM) to detect corrosion damage on the morphologies of Al foil after CA experiments (Fig. 2C, D). The determined Al contents of the electrolyte with Li₃PO₄ or Li₂CO₃ reached 0.67 and 1.8 ppm, respectively, which are considerably lower than that of in blank 1 m LiTFSI (46.29 ppm). In addition, the corrosive

pits were scarce and tiny compared with those of Al foil in 1 m LiTFSI. Furthermore, the cycled Al foils in 1 m LiTFSI with additives were washed in ethanol to prevent residual electrolyte from occupying their surface and immersed in 1 m LiTFSI to repeat the CA experiment under the same condition. The foils still exhibited an excellent anticorrosion

effect with a low corrosive current density (Figure S3) and low content of dissolved Al (Li_3PO_4 : 0.46 ppm, LiAlO_2 : 0.73 ppm, Li_2CO_3 : 1.19 ppm, and Li_2SiO_3 : 2.26 ppm; Fig. S4). Thus, a passivation layer formed in the first round of the CA experiment by HTA. Moreover, the passivation layer provided a robust and continuous protection to the Al foil in pure 1 m LiTFSI.

Additional corrosion experiments were conducted in 10 m LiTFSI to align with the concentrations used in actual battery systems. Ti serves as a highly corrosion-resistant current collector in aqueous batteries³⁶. Compared with Ti, Al foils with Li_3PO_4 ($2.35 \times 10^{-6} \text{ A cm}^{-2}$) and Li_2CO_3 ($2.71 \times 10^{-6} \text{ A cm}^{-2}$) exhibit the same order of magnitude of corrosion current density as Ti ($5.34 \times 10^{-6} \text{ A cm}^{-2}$; Figs. 2B and S8). Li_2CO_3 and Li_3PO_4 are considered much better anti-corrosion additives than Li_2SiO_3 ($3.56 \times 10^{-5} \text{ A cm}^{-2}$), whose corrosion current density is lower by one order of magnitude than Li_2SiO_3 . Evidently, the ICP revealed that the 10 m LiTFSI with Li_2CO_3 failed to detect the Al signal due to lower value than the detection minimum. The value for Li_3PO_4 was 0.05 ppm, which is considerably lower than that of Li_2SiO_3 (7.56 ppm). Such result was probably due to the substantial change in pH from 6.82 (10 m LiTFSI), 6.87 (10 m LiTFSI + Li_2CO_3), 6.93 (10 m LiTFSI + Li_3PO_4) to 9.20 (10 m LiTFSI + Li_2SiO_3 ; Fig. S2). Thus, in the following section, we focused on the HTAs (Li_2CO_3 and Li_3PO_4) in 10 m LiTFSI and evaluated their electrochemical performance.

XPS was conducted to detect the passivation layer that formed on the Al foils after the introduction of HTA (Fig. 2E). Considering the insulating Al_2O_3 on pristine Al foils, we used its XPS spectrum as a reference (Al_2O_3 , Al 2p: 74.81 eV). $\text{Al}(\text{OH})_3$ was detected at 74.37 eV for Li_3PO_4 , 74.27 eV for Li_2CO_3 , and 74.19 eV for Li_2SiO_3 (Fig. 2E), consistent with the reported value in literature (74.4 eV)³⁷. This finding indicates that the Al^{3+} originating from the oxidation of Al interacted with the anions of HTAs (HPO_4^{2-} , H_2PO_4^- , HCO_3^- , and HSiO_3^-) and was hydrolyzed to insoluble solid $\text{Al}(\text{OH})_3$ to form the passivation film that covered the active corrosion spots on the Al surface film and blocked further corrosive reaction. To further clarify our claims, we compared the pristine samples with their corresponding Ar^+ sputtering samples. The blank 10 m LiTFSI showed asymmetric double Al 2p peaks belonging to the metallic Al foil, which indicates the destruction of pristine Al_2O_3 film and its failure to exert anticorrosion action against the aqueous LiTFSI electrolyte. By contrast, for the HTAs observed after 60 s Ar ion sputtering, signals from the passivation layers $\text{Al}(\text{OH})_3$ weakened, but remained with a relatively high intensity. Specifically, during etching, the signals of pristine Al_2O_3 intensified, which signifies the presence of double passivation layers consisting of an $\text{Al}(\text{OH})_3$ top layer and a pristine Al_2O_3 bottom layer. Thus, ceaseless destruction of the Al_2O_3 layer by TFSI was impossible due to the passivation of Al foil because once the corrosion pitting sites appeared, the dissolved Al^{3+} rapidly reacted with the HTA, which resulted in $\text{Al}(\text{OH})_3$ layer covering the undamaged Al_2O_3 layer around the pitting site. Based on the information mentioned above, a compact and stable passivation layer $\text{Al}(\text{OH})_3$ formed on the surface of Al foil. Moreover, we observed our proposed mechanism in aqueous sodium-ion electrolytes, in which Na_2CO_3 exhibited an effective anticorrosion effect on the Al foil (Figs. S8–S10). Thus, our concept is universal and applies to the stabilization of Al foils in aqueous batteries.

Identification and quantification of Al oxidation corrosion for electron supplement

During corrosion, the current collector provided additional irreversible overcharging capacity as a result of Al oxidation. In consideration of the charge balance of batteries, Al oxidation at the cathode side corresponded to the reduction on the anode side, which balanced the redox reaction. Thereby, in such a redox reaction, the prelithiation of the anode compensates for the extra electron loss on the cathode side. To verify the life extension mechanism via Al oxidation, we evaluated individual Al and Ti current collectors in a full cell (LMO || 10 m LiTFSI ||

TiO , P/N = 2) (Fig. 3). An extra 2 cm^2 bare Al foil was attached behind the 0.79 cm^2 LiMn_2O_4 electrode to amplify electron supplementation via the oxidation of Al as a prelithiation additive. Figure 3 reveals that compared with the Ti current collector, the battery with an Al current collector exhibited an extra plateau of around 1.2–1.3 V at the first charge process, and such finding was attributed to the corrosion of the Al current collector. Moreover, the extra plateau of approximately 1 V at the following discharge process belongs to the overlithiation of LiMn_2O_4 . This result indicates the corrosive oxidation of the Al current collector at the earlier stage of the first charge, accompanied with the intercalation of Li ions in TiO_2 . This condition resulted in the partial prelithiation of the anode (Li_xTiO_2) and overlithiation of $\text{Li}_{1-x}\text{Mn}_2\text{O}_4$ in the following discharge (Fig. 3B). Overall, Al was oxidized into Al ions that were dissolved in the electrolyte. In addition, Li ions from the electrolyte were intercalated in the active material. The electrolyte served as an additional source of lithium, and oxidation of the Al foil was the extra electron supplement. Thus, oxidation of Al current collectors at the cathode side can function as a prelithiation additive to prolong the life of batteries.

Despite the prelithiation via the oxidation of the current collector, the feasibility of electrochemical regulation of corrosion and passivation requires further verification before a proof of concept can be proposed. Suppose the corrosion process cannot be controlled through electrochemical regulation. In such a case, the electrode will be damaged, and continuous irreversible overcharging will overcompensate for the fully lithiated $\text{Li}_{0.5}\text{TiO}_2$, which will result in the low utilization of capacity and further acceleration of other parasitic reactions, such as HER. Such condition will lead to the degradation of the battery's lifespan. Fortunately, this problem can be solved with the use of HTA. A small amount of Al has to be corroded first to offer some dissolving Al ion as the reaction source for the following passivation by HTA. Such a mechanism ensures the electrochemical regulation of the corrosion–passivation of Al for the long-term cycle life of battery via the stabilization of the Al current collector and appropriate supplementation of lithium loss.

To further confirm that the oxidation of Al only prelithiates the anode in the initial charge process and the passivated Al by HTA serves as a robust current collector in the following cycle, we designed three-electrode cells with two fresh TiO_2 anodes to distinguish Al oxidation in the first and second cycles and an excess LiMn_2O_4 cathode with a high P/N ≈ 3 to provide sufficient lithium resource to sustain the

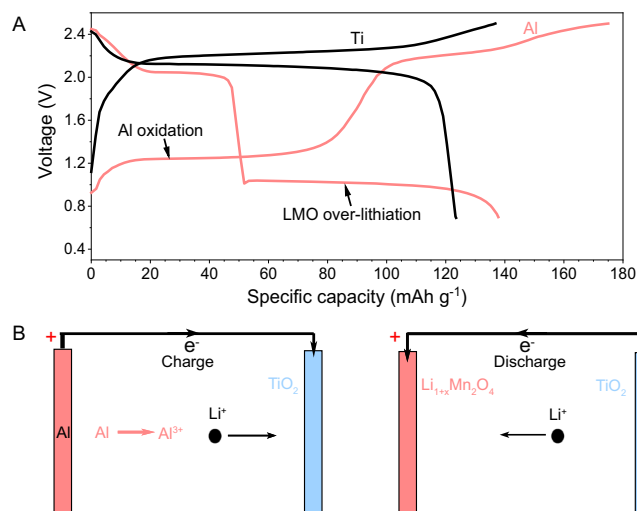


Fig. 3 | Identification of Al oxidation corrosion for electron supplement. A First charge–discharge profiles of LiMn_2O_4 – TiO_2 cells with Al or Ti current collector in 10 m LiTFSI. **B** Schematic of the prelithiation of TiO_2 via Al current collector oxidation in the charge process and overlithiation of LiMn_2O_4 in the discharge process.

double TiO_2 anodes (Fig. 4A). Accordingly, the charging program of batteries was set up in the following order: (1) cell configuration: LMO electrode / TiO_2 electrode, first full charging at 1 C; (2) cell configuration: LMO electrode / TiO_2 electrode, second full charging at 1 C rate. As the entire process occurred without discharging, interference was eliminated from overlithiation of LiMn_2O_4 . As shown in Fig. 4B, regardless of whether Li_3PO_4 and Li_2CO_3 was used, the Al oxidation occurred at approximately 1.2 V on the first charge and almost disappeared on the second charge (Li_2CO_3 : 1st 59.34 mAh g^{-1} and 2nd 2.73 mAh g^{-1} ; Li_3PO_4 : 1st 77.22 mAh g^{-1} and 2nd 9.68 mAh g^{-1}). Thus, the corrosion and passivation with the aid of additives mainly transpired during the first charge, accompanied by the electron supplement from the Al oxidation. In the following cycles, the Al current collector was stabilized via passivation to support the long-term calendar life of aqueous batteries.

Effectiveness of HTA in prolonging the cycle life of batteries

We assembled LiMn_2O_4 || TiO_2 full cells ($P/N \approx 2$) to evaluate the effectiveness of Li_3PO_4 and Li_2CO_3 additives (Fig. 5). The Al and Ti current collectors with a blank electrolyte consisting of 10 m LiTFSI served as control samples. To magnify the passivation process and the effects of electron supplement from Al oxidation, we attached an extra Al foil (2 cm^2) behind the LiMn_2O_4 electrode (0.79 cm^2), excluding the Ti current collector. As shown in Fig. 5A, Al corrosion commenced at approximately 1.2 V, along with Al passivation by HTA, which reflects an increase in the plateau from 1.2 V to 1.4 V, consistent with the peak of -1.3 V in the dQ/dV plot (Fig. 5B). Furthermore, full cells can survive in the relatively low-concentration electrolyte (10 m LiTFSI) with HTAs, whose cycle life improved substantially from 12.6% to above 84.7% (Li_2CO_3) and 89.1% (Li_3PO_4) after 1500 times. Such result was due to the

suppressed continuously irreversible Al corrosion via passivation, which maintained the good electronic conducting contact between the electrode and current collector. In addition, the cycling stability of anticorrosion Ti (65.2%, 1500 cycles) cannot surpass that of Al with HTA, which confirms the effect of the prelithiation of TiO_2 during electrochemical-chemical Al passivation. Figure 5D indicates a clear distinction between the efficiency of cells with and without additives. Batteries with HTA showed a rapid increase in efficiency at the initial cycles, with 1500 cycles average values of 99.36% (Li_2CO_3) and 99.37% (Li_3PO_4), which are considerably higher than that of 10 m LiTFSI (98.03%). Thus, the electrochemical-chemical Al passivation derived by HTA can stabilize the Al current collector in relatively low-concentration electrolytes and offer an electron supplement for the prolonged cycle life of ALIBs.

Prototype of SP-ALIBs

From a practical point of view, as the mass loading of commercial Li-ion batteries reaches above 20 mg cm^{-2} . Given the limited reactive mass of the Al current collector, the effectiveness of electron supplement from the Al current collector alone may be extremely low in actual conditions. To solve this problem, we designed a new battery type through introduction of an Al sacrificial prelithiation electrode dedicated to being oxidized as the electron supplement (Fig. 6B). The detailed program is as follows. Prior to cycling, the cell was pre-charged with an Al sacrificial prelithiation electrode to obtain TiO_2 anode partially prelithiated (Al || TiO_2). The prelithiation capacity of TiO_2 is depicted with the red short bar in Fig. 6A. Subsequently, the LiMn_2O_4 electrode, instead of the sacrificial Al electrode, initiated the cycling process (LiMn_2O_4 || TiO_2). As shown in Fig. 6A, when TiO_2 was fully lithiated by LiMn_2O_4 , the quantity of Li extracted from LiMn_2O_4

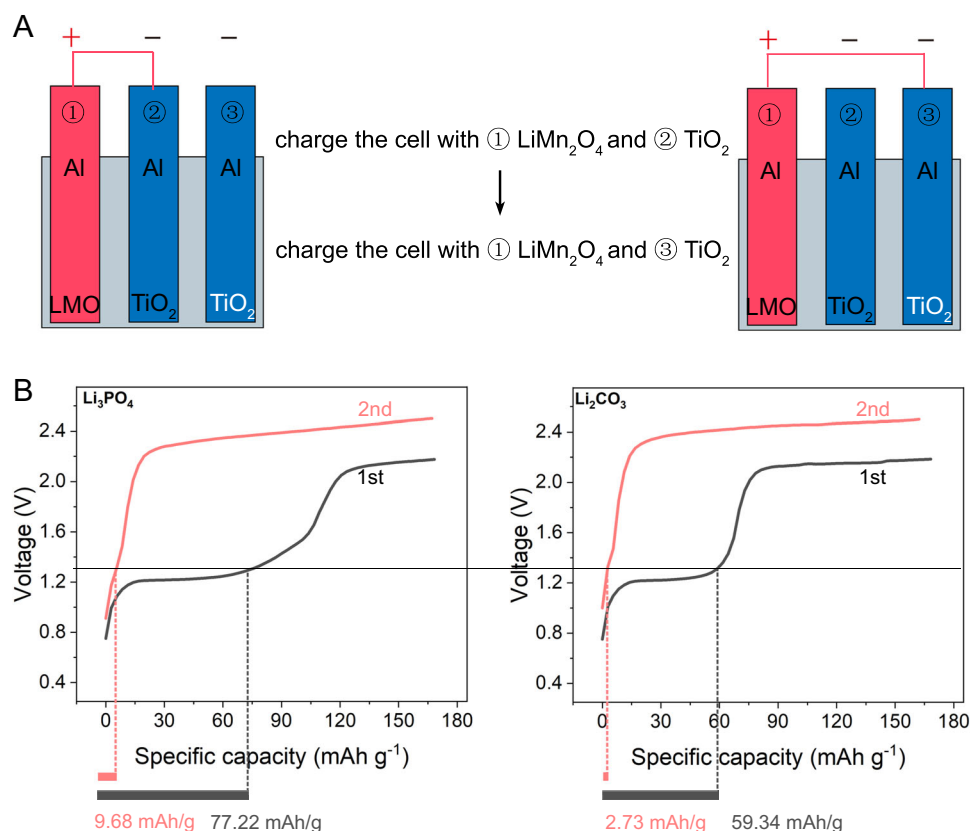


Fig. 4 | Duration of Al oxidation corrosion for electron supplement. **A** Process diagram for continuous charging of dual-anode battery. Charge the battery with LiMn_2O_4 cathode and TiO_2 anode, then charge it with LiMn_2O_4 cathode and TiO_2

TiO_2 anode. **B** Consecutive charging profiles of batteries with one LiMn_2O_4 cathode and two TiO_2 anodes in 10 m LiTFSI + Li_2CO_3 or Li_3PO_4 .

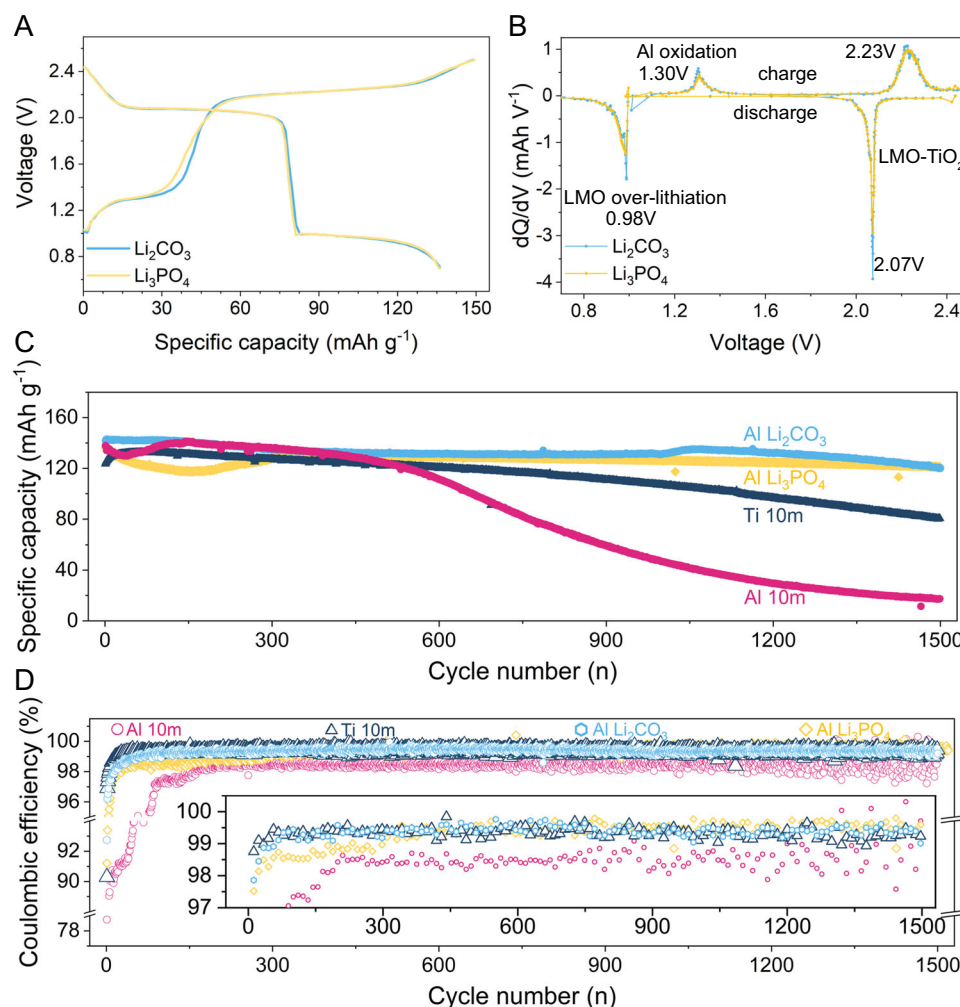


Fig. 5 | Cycling performance of ALIBs with Li_2CO_3 and Li_3PO_4 additives. A, B First charge–discharge profiles and dQ/dV curves of $\text{LiMn}_2\text{O}_4 \parallel \text{TiO}_2$ cells with an Al current collector in 10 m LiTFSI with additives. **C** Cycling stability of $\text{LiMn}_2\text{O}_4 \parallel \text{TiO}_2$

cells with Al and Ti current collectors in 10 m LiTFSI with/without additives. **D** Comparison of coulombic efficiency with a magnified view inside.

during the charging process was less than the Li extracted from TiO_2 during the discharging process, which caused the overlithiation of LiMn_2O_4 . Overall, Al is a controllable electron supplement. In addition to the initial stage, when capacity faded after long cycles, the cathode can be switched to an Al electrode for another electron supplementation. Preliminarily, we constructed a pouch cell (Al || LiMn_2O_4 -Ti || TiO_2) employing a Ti current collector to clarify the extra electron supplement only from the sacrificial prelithiation Al electrode (Figure S15). The anode was initially prelithiated using a sacrificial prelithiation Al electrode (2.4 V constant potential between Al and TiO_2 for 20 minutes at 25 °C), which corresponded to the new discharge plateau of 0.98 V with an overlithiation capacity of 26.7 mAh g^{-1} and subsequently resulted in notably better cycling performance. Finally, we constructed a 0.5 Ah multilayer stacked SP-ALIBs with Al foil as the current collector (Al || LiMn_2O_4 -Al || TiO_2 , 0.5 Ah, and 55.2 Wh kg^{-1}), whose loading mass was 20 mg cm^{-2} for LiMn_2O_4 and 12 mg cm^{-2} for TiO_2 , which are close to the level of commercial Li-ion batteries. The introduction of the sacrificial Al electrode lowered the energy density. However, as the sacrificial Al electrode had a high theoretical capacity of 2980 mAh g^{-1} , the overall estimated energy density decreased by less than 5%. After the prelithiation of TiO_2 anode by the Al electrode (2.8 V constant potential between Al and TiO_2 for 22 h at 35 °C), the discharge profile of the initial cycle showed the overlithiation plateau of LiMn_2O_4 (Fig. 6C). This finding reveals that high voltage and temperature cause the

partial destruction of the passivation layer on sacrificial prelithiation Al electrodes generated by HTA and the feasibility of using applied potential and temperature to regulate Al corrosion with time. For the simultaneous protection of the Al current collector and utilization of Al corrosion for electron supplement, an additional sacrificial Al electrode was used, and the operating conditions of the Al current collector and sacrificial electrode were differentiated. In this case, the Al current collector was protected from HTA and functioned well throughout the battery lifespan. Meanwhile, the sacrificial Al electrode was oxidized in harsh conditions to prelithiate TiO_2 . The capacity retention of SP-ALIBs with HTA (Li_2CO_3) rose to 70.1% after 200 cycles, which is considerably higher than that of the traditional $\text{LiMn}_2\text{O}_4 \parallel \text{TiO}_2$ cell without HTA (49.5%) (Fig. 6D).

Furthermore, a distinct coulombic efficiency difference was observed between SP-ALIBs (average 99.32% for 200 cycles) and normal cells (93.14%). The low efficiency was attributed to the failure of the Al current collector at the cathode and electrolyte pollution by Al^{3+} . Thus, the HTA must convert the corrosion product Al^{3+} to precipitate it as a passivation layer. We validated the reliability of our design through the assembly and evaluation of three SP-ALIBs (0.5 Ah) to (Fig. S17), which showed an excellent consistency. The prototype of SP-ALIBs achieved the stability of Al current collectors in harsh aqueous environments and supplemented extra electrons via the sacrificial prelithiation Al electrode, which has great potential for industrial application. An open design for electrolyte replenishment should be

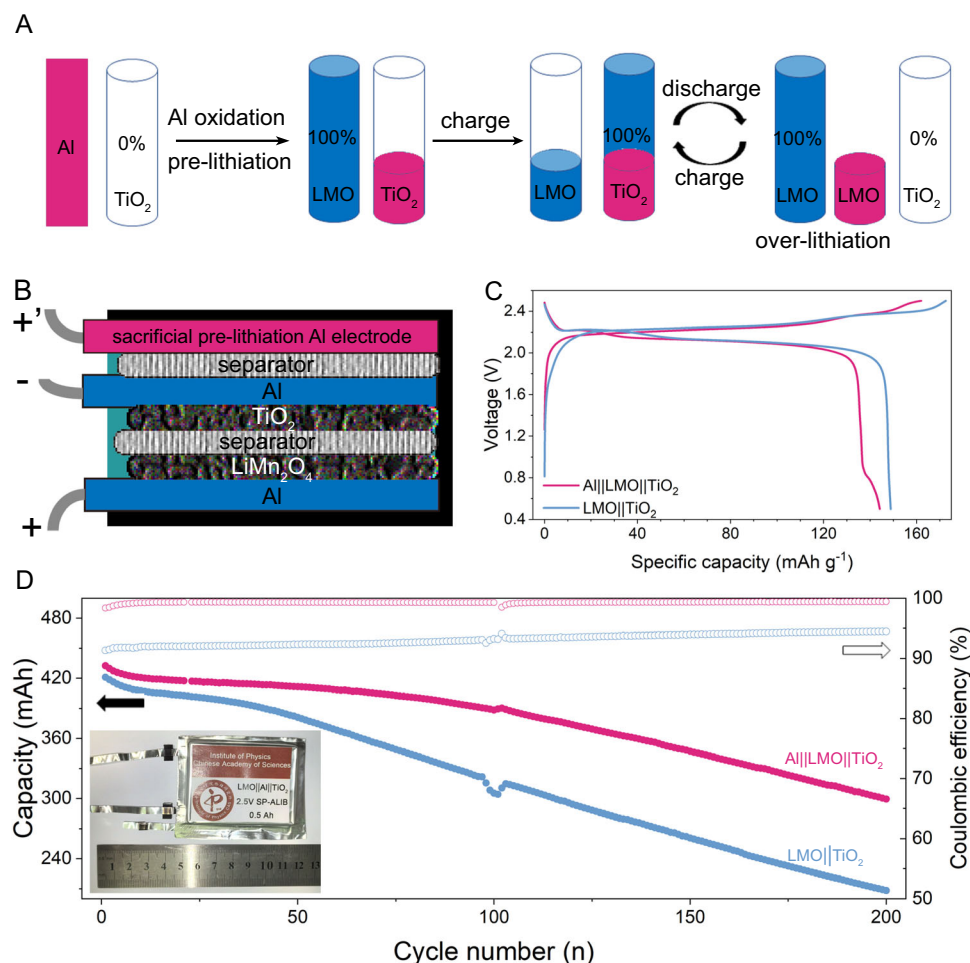


Fig. 6 | Prototype of SP-ALIBs (Al||LiMn₂O₄||TiO₂). **A** Program for SP-ALIBs. **B** Schematic of SP-ALIBs. **C** First charge–discharge profiles of the formation process of the 0.5 Ah SP-ALIB at 0.8 C after the prelithiation of TiO₂ anode at 2.8 V for 22 h

via the sacrificial prelithiation Al electrode and traditional pouch cell. **D** Comparison of cycle stabilities of SP-ALIBs and traditional pouch cell at 1 C rate. Inset: photo of a practical SP-ALIB.

considered for practical purposes due to electrolyte loss during long-term cycling.

Discussion

In this work, the anticorrosion effectiveness of HTAs was discovered, and their mechanism was investigated. With the assistance of HTA, a robust Al(OH)₃ passivation layer formed on the Al surface, which dramatically lowered the corrosion current density by nearly three orders of magnitude (10⁻⁶ A cm²) in 1 m LiTFSI solution. Such a condition made the Al foil corrosion-resistant and comparable to Ti. Moreover, through regulation by HTA, the controllable electrochemical corrosion process on the cathode side can be used to prelithiate the anode. With the robust Al current collector and extra electron supplemented by Al passivation, full cells can survive in relatively low-concentration electrolytes (10 m LiTFSI) with the employment of HTA, whose cycle life improved substantially from 12.6% to above 84.7% (Li₂CO₃) and 89.1% (Li₃PO₄) after 1500 times. Such finding implies the feasibility of using Al corrosion–passivation regulation to prolong the life of aqueous batteries. Al passivation ensured that the current collector's long-term chemical/electrochemical stability and Al oxidation corrosion compensated for the irreversible capacity loss caused by HER and SEI formation. Based on these results, we designed a prototype of SP-ALIBs with an extra Al sacrificial prelithiation electrode as an electron supplement. The capacity retention of the 0.5 Ah prelithiated SP-ALIBs with HTA (Li₂CO₃) rose to 70.1% at 1C after 200 cycles, and such value is higher

than that of the traditional LiMn₂O₄ || TiO₂ cell (49.5%). The average efficiency increased from 93.14% to 99.32%. The discovery of HTA in a broader context revealed the once-overlooked complicated corrosion and passivation processes that occur in batteries in general. Through exploration of anticorrosion additives, the SP-ALIBs will gain more potential to achieve long-life ALIBs, which benefits the sustainable and lifelong industrial applications of ALIB.

Methods

Preparation of LiMn₂O₄-TiO₂, LiMn₂O₄-TiO₂-TiO₂, Al-TiO₂, and LiMn₂O₄-Al-TiO₂ pouch cells

All pouch cells other than 0.5 Ah were assembled using a glass fiber as a separator, 10 m LiTFSI as the electrolyte (some with HTA), and Al plastic film as packaging. We fabricated the LiMn₂O₄ cathode by mixing LiMn₂O₄, carbon black (CB), and polyvinylidene fluoride (PVDF) at a weight ratio of 8:1:1 in N-methyl pyrrolidinone (NMP) in an SK-300SII CE mixing machine (SHASHIN KAGAKU Co., Ltd.) for 20 minutes at a speed of 2000 rsm to produce a black slurry. The slurry was spread uniformly on a clean Al or Ti foil and then dried. TiO₂ anode was prepared using the same process and spread on the Al foil using the same CB, PVDF, and NMP at a weight ratio of 8:1:1. An extra 2 cm² bare Al foil was attached behind the Al current collectors of LiMn₂O₄ in Figure 345 aside from LiMn₂O₄ with Ti current collector. The small pouch cells included unilaterally coated LiMn₂O₄ cathode (diameter: 10 mm, thickness: ~41.2 μm, and mass loading: ~3.2 mg cm⁻²), unilaterally coated TiO₂ anode (diameter: 10 mm, thickness ~29 μm, and

mass loading -1.6 mg cm^{-2}), and separator (area $2.5 \text{ cm} \times 1.3 \text{ cm}$; thickness: $\sim 55 \text{ }\mu\text{m}$). The 10 m LiTFSI was used as an electrolyte. HTA was added to the electrolyte as an additive until saturation and the supernatant was used in the pouch cells. Li_2CO_3 , Li_3PO_4 , Li_2SiO_3 , or LiAlO_2 was hard to dissolve in 10 m LiTFSI, and saturation was reached at a concentration below 0.05 m.

The 0.5 Ah SP-ALIBs were assembled with eight layers of LiMn_2O_4 cathode, seven layers of TiO_2 anode, and a sacrificial Al electrode. LiMn_2O_4 and TiO_2 had mass loadings of -20 (90 wt%) and -12 mg cm^{-2} (80 wt%), respectively. The cathode area was $4.5 \text{ cm} \times 5.8 \text{ cm}$, that of the anode was $4.3 \text{ cm} \times 5.6 \text{ cm}$, and the width of the PP separator was 6 cm. The sacrificial Al electrode ($4.5 \text{ cm} \times 5.8 \text{ cm}$) was sanded using a sandpaper to facilitate corrosion and placed on one side of the cell. Prior to standard formation, the sacrificial Al electrode prelithiated the cell at a constant voltage of 2.8 V at $35 \text{ }^\circ\text{C}$ for 22 h.

The electrolyte in this study was consistently expressed in terms of molality (m).

Electrochemical measurements

CA experiments were conducted in a $25 \text{ }^\circ\text{C}$ constant-temperature chamber using CHI 660E electrochemical workstation in three-electrode cells with 10 mL electrolyte, and the area of the Al working electrode was 1 cm^2 . The CA experiments on LiTFSI solution were performed in three-electrode devices (Al-WE || Ag/AgCl-RE || Al-CE), where the potential of the Al-WE was set at 4.5 V vs Li/Li⁺ for 10 minutes, relaxed to the OCV for 1 minutes, and cycled for 12 times as above. The batteries were tested using a LAND battery test system (Wuhan, China). The pouch cells in Figs. 3 and 5 were tested at the 3 C rate, and those in Figs. 4 and 6 were tested at a 1 C rate. The small pouch cells in Figs. 3, 4, and 5 had a cutoff voltage from 0.7 V to 2.5 V. The 0.5 Ah pouch cells in Fig. 6 experienced a cutoff voltage of 0.5 V to 2.5 V. All batteries were tested in a $25 \text{ }^\circ\text{C}$ constant-temperature chamber. Calculations of the specific energy of 0.5 Ah pouch cells was based on the masses of the cathode, anode, separator, and electrolyte.

Characterizations

SEM images of the morphologies of the Al foil after CA experiments were obtained using a Hitachi S-4800 field-emission scanning electron microscope operated at 10 kV. XPS analysis was performed using an ESCALAB 250 Xi, ThermoFisher with Mg/Al K α radiation. All the binding energies were referenced to the C 1s line at 284.8 eV. All electrolyte contents were measured on an ICP-OES Agilent 5800.

Reporting summary

Further information on research design is available in the Nature Portfolio Reporting Summary linked to this article.

Data availability

Source data are provided in this paper. Extra data are available from the corresponding author upon reasonable request. Source data are provided with this paper.

References

- Li, W., Dahn, J. R. & Wainwright, D. S. Rechargeable lithium batteries with aqueous electrolytes. *Science* **264**, 1115–1118 (1994).
- Wang, Y., Yi, J. & Xia, Y. Recent progress in aqueous lithium-ion batteries. *Adv. Energy Mater.* **2**, 830–840 (2012).
- Suo, L. et al. Water-in-salt[†] electrolyte enables high-voltage aqueous lithium-ion chemistries. *Science* **350**, 938–943 (2015).
- Liu, B. et al. Sandwich structure corrosion-resistant current collector for aqueous batteries. *ACS Appl. Energy Mater.* **4**, 4928–4934 (2021).
- Yue, J. & Suo, L. Progress in rechargeable aqueous alkali-ion batteries in China. *Energy Fuels* **35**, 9228–9239 (2021).
- Kühnel, R. S. et al. Water-in-salt[†] electrolytes enable the use of cost-effective aluminum current collectors for aqueous high-voltage batteries. *Chem. Commun.* **52**, 10435–10438 (2016).
- Ratajczak, P., Jurewicz, K., Skowron, P., Abbas, Q. & Béguin, F. Effect of accelerated ageing on the performance of high voltage carbon/carbon electrochemical capacitors in salt aqueous electrolyte. *Electrochim. Acta* **130**, 344–350 (2014).
- Zhou, X., Peng, C. & Chen, G. Z. 20 V stack of aqueous supercapacitors with carbon (–), titanium bipolar plates and CNT-polypyrrole composite (+). *AIChE J.* **58**, 974–983 (2012).
- Wen, Y. H. et al. Carbon coated stainless steel mesh as a low-cost and corrosion-resistant current collector for aqueous rechargeable batteries. *J. Mater. Chem. A* **5**, 15752–15758 (2017).
- Guo, L., Thornton, D. B., Koronfel, M. A., Stephens, I. E. L. & Ryan, M. P. Degradation in lithium ion battery current collectors. *J. Phys. Energy* <https://doi.org/10.1088/2515-7655/ac0c04> (2021).
- Liu, S., Ye, S. H., Li, C. Z., Pan, G. L. & Gao, X. P. Rechargeable aqueous lithium-ion battery of $\text{TiO}_2/\text{LiMn}_2\text{O}_4$ with a high voltage. *J. Electrochem. Soc.* <https://doi.org/10.1149/2.094112jes> (2011).
- Zhao, M., Huang, G., Zhang, B., Wang, F. & Song, X. Characteristics and electrochemical performance of $\text{LiFe}_0.5\text{Mn}_0.5\text{PO}_4/\text{C}$ used as cathode for aqueous rechargeable lithium battery. *J. Power Sources* **211**, 202–207 (2012).
- Dyatkin, B. et al. Development of a green supercapacitor composed entirely of environmentally friendly materials. *ChemSusChem* **6**, 2269–2280 (2013).
- Lahan, H. & Das, S. K. Active role of inactive current collector in aqueous aluminum-ion battery. *Ionics* **24**, 2175–2180 (2018).
- Luo, W. et al. Highly conductive, light weight, robust, corrosion-resistant, scalable, all-fiber based current collectors for aqueous acidic batteries. *Adv. Energy Mater.* **8**, 6 (2018).
- Yao, Y. G. et al. Epitaxial welding of carbon nanotube networks for aqueous battery current collectors. *ACS Nano* **12**, 5266–5273 (2018).
- Ziv, B. et al. Investigation of graphite foil as current collector for positive electrodes of Li-ion batteries. *J. Electrochem. Soc.* **160**, A581–A587 (2013).
- Wang, X., Yasukawa, E. & Mori, S. J. E. A. Inhibition of anodic corrosion of aluminum cathode current collector on recharging in lithium imide electrolytes. *Electrochim. Acta* **45**, 2677–2684 (2000).
- Kawamura, T. et al. Methyl difluoroacetate inhibits corrosion of aluminum cathode current collector for lithium ion cells. *Electrochem. Solid-State Lett.* **8**, A459 (2005).
- Piao, N., Wang, L. & He, X. J. Anodic stabilities of various metals as the current collector in high concentration electrolytes for lithium batteries. *J. Electrochem. Soc.* **168**, 030509 (2021).
- McOwen, D. W. et al. Concentrated electrolytes: decrypting electrolyte properties and reassessing Al corrosion mechanisms. *Energy Environ. Sci.* **7**, 416–426 (2014).
- Matsumoto, K. et al. Suppression of aluminum corrosion by using high concentration LiTFSI electrolyte. *J. Power Sources* **231**, 234–238 (2013).
- Nakajima, T., Mori, M., Gupta, V., Ohzawa, Y. & Iwata, H. Effect of fluoride additives on the corrosion of aluminum for lithium ion batteries. *Solid State Sci.* **4**, 1385–1394 (2002).
- Song, S.-W., Richardson, T. J., Zhuang, G. V., Devine, T. M. & Evans, J. W. Effect on aluminum corrosion of LiBF_4 addition into lithium imide electrolyte; a study using the EQCM. *Electrochim. Acta* **49**, 1483–1490 (2004).
- Yan, G. et al. Lithium difluoro(oxalato)borate as an additive to suppress the aluminum corrosion in lithium bis(fluorosulfonyl)imide-based nonaqueous carbonate electrolyte. *J. Solid State Electrochem.* **20**, 507–516 (2016).
- Yang, H., Kwon, K., Devine, T. M. & Evans, J. W. J. Aluminum corrosion in lithium batteries an investigation using the

- electrochemical quartz crystal microbalance. *J. Electrochem. Soc.* **147**, 4399 (2000).
27. Krause, L. J. et al. Corrosion of aluminum at high voltages in non-aqueous electrolytes containing perfluoroalkylsulfonyle imides; new lithium salts for lithium-ion cells. *J. Power Sources* **68**, 320–325 (1997).
 28. Morita, M., Shibata, T., Yoshimoto, N. & Ishikawa, M. Anodic behavior of aluminum current collector in LiTFSI solutions with different solvent compositions. *J. Power Sources* **119–121**, 784–788 (2003).
 29. Theivaprakasam, S. et al. Passivation behaviour of aluminium current collector in ionic liquid alkyl carbonate (hybrid) electrolytes. *npj Mater. Degrad.* <https://doi.org/10.1038/s41529-018-0033-6> (2018).
 30. Ding, R. et al. Recent advances in cathode prelithiation additives and their use in lithium-ion batteries. *J. Electroanal. Chem.* <https://doi.org/10.1016/j.jelechem.2021.115325> (2021).
 31. Huang, Z. et al. Progress and challenges of prelithiation technology for lithium-ion battery. *Carbon Energy* **4**, 1107–1132 (2022).
 32. Lv, T. & Suo, L. Water-in-salt widens the electrochemical stability window: thermodynamic and kinetic factors. *Curr. Opin. Electrochem.* <https://doi.org/10.1016/j.coelec.2021.100818> (2021).
 33. Szklarska-Smialowska, Z. J. C. Pitting corrosion of aluminum. *Corros. Sci.* **41**, 1743–1767 (1999).
 34. Rudd, W. J. & Scully, J. C. The function of the repassivation process in the inhibition of pitting corrosion on aluminium. *Corros. Sci.* **20**, 611–631 (1980).
 35. Buchheit, R. G., Bode, M. D. & Stoner, G. E. Corrosion-resistant, chromate-free talc coatings for aluminum. *Corrosion* **50**, 205–214 (1994).
 36. Giurlani, W. et al. Electrochemical stability of steel, Ti, and Cu current collectors in water-in-salt electrolyte for green batteries and supercapacitors. *J. Solid State Electrochem.* **26**, 85–95 (2022).
 37. Rueda, F. et al. Characterization of Venezuelan laterites by X-ray photoelectron spectroscopy. *J. Electron. Spectrosc. Relat. Phenom.* **82**, 135–143 (1996).

Acknowledgements

This work was supported by the National Key Research and Development Program of China (2022YFB2404500), the National Natural Science Foundation of China (U22B20124), CAS Youth Interdisciplinary Team, and the Center for Clean Energy.

Author contributions

L.S. conducted the project. B.L. and L.S. conceived the concept and designed this work. B.L. and L.S. wrote the paper. B.L. conducted the

electrochemical experiments, SEM, and ICP measurements. T.L. (Tianshi Lv) conducted the XPS measurements. T.L. (Tianshi Lv), A.Z. and X.Z. participated in constructing the 0.5Ah batteries. Z.L. participated in drawing the schematic diagram. T.L. (Ting Lin) assisted in analyzing the composition of the passivation layer. All authors participated in the analysis of the results and reviewed the manuscript.

Competing interests

The authors declare no competing interests.

Additional information

Supplementary information The online version contains supplementary material available at <https://doi.org/10.1038/s41467-024-47145-3>.

Correspondence and requests for materials should be addressed to Liumin Suo.

Peer review information *Nature Communications* thanks the anonymous reviewer(s) for their contribution to the peer review of this work. A peer review file is available.

Reprints and permissions information is available at <http://www.nature.com/reprints>

Publisher's note Springer Nature remains neutral with regard to jurisdictional claims in published maps and institutional affiliations.

Open Access This article is licensed under a Creative Commons Attribution 4.0 International License, which permits use, sharing, adaptation, distribution and reproduction in any medium or format, as long as you give appropriate credit to the original author(s) and the source, provide a link to the Creative Commons licence, and indicate if changes were made. The images or other third party material in this article are included in the article's Creative Commons licence, unless indicated otherwise in a credit line to the material. If material is not included in the article's Creative Commons licence and your intended use is not permitted by statutory regulation or exceeds the permitted use, you will need to obtain permission directly from the copyright holder. To view a copy of this licence, visit <http://creativecommons.org/licenses/by/4.0/>.

© The Author(s) 2024